




Deformation and hyperon halo in hypernuclei

Huai-Tong Xue (薛怀通) , Q. B. Chen (陈启博) , Xian-Rong Zhou (周先荣) ,* and Y. Y. Cheng (程奕源)
Department of Physics, East China Normal University, Shanghai 200241, China

H.-J. Schulze 

INFN Sezione di Catania, Dipartimento di Fisica, Università di Catania, Via Santa Sofia 64, 95123 Catania, Italy



(Received 6 April 2022; accepted 13 September 2022; published 10 October 2022)

The effects of deformation and the change of the nuclear core on the hyperon binding and halo structure in single- Λ p -shell hypernuclei are studied for the C hyperisotopes and $N = 6$ hyperisotones in the framework of the deformed Skyrme-Hartree-Fock approach with combinations of the NN interactions SIII, SGII, SkI4 and the ΛN interactions LY1 and SLL4, respectively. Deformation causes more deeply bound states with smaller extension of the density distributions and radii. The possibility of deformed halo structures of Λ $1p$ states in hypernuclei up to a mass number $A = 15$ is found.

DOI: [10.1103/PhysRevC.106.044306](https://doi.org/10.1103/PhysRevC.106.044306)

I. INTRODUCTION

Since the observation of the neutron halo structure in ^{11}Li in 1985 [1], the halo phenomenon has been intensively studied from both experimental and theoretical sides [2–4] in very neutron-rich nuclei, which are far away from the valley of stability, close to or at the neutron drip line. Compared to their isobars, the neutron density distribution of halo nuclei can extend far beyond the nuclear surface area and they have an abnormally large matter radius. In addition, halo nuclei can have strong soft electric dipole transition strengths [5]. Necessary conditions for forming a halo are that one or two valence neutrons have (a) weak binding with typical separation energies $S_n \lesssim 1$ MeV [3,6], which are significantly smaller than the canonical value of 8 MeV and (b) low orbital angular momenta $l = 0$ or 1 [3]. The binding of one or two valence neutrons is so loose that they can tunnel deeply into the classical prohibited area and hence form an extensively diffused halo surrounding the compact core of the nucleus [7].

Some neutron halo states have been discovered for sd -shell neutron-rich nuclei, e.g., the Ne isotopes [8]. In these systems, structures with large quadrupole deformation β_2 have been observed [9,10]. One or two neutrons from the previously described nuclei will contribute to the formation of the halo structure. For heavier nuclei, such as neutron-rich Ca and Zr isotopes, a giant halo phenomenon was predicted in Refs. [11,12], in which multiple neutrons participate in the formation of halo structure.

Since the discovery of the first hyperfragment in an emulsion exposed to cosmic rays in 1953 [13], hypernuclei have been investigated extensively both theoretically and experimentally to understand the hyperon-nucleon (YN) and hyperon-hyperon (YY) interactions. The Λ hypernucleus, composed of ordinary nuclear core and the lightest hyperon

Λ , provides a unique laboratory to study the ΛN interactions. Because unrestricted by the Pauli exclusion principle, the Λ hyperon can enter deeply into the nucleus and is a good probe to study the nuclear structure and interaction that would be more obscured in ordinary nuclei.

So far, numerous studies have been conducted on the influence of the hyperon in neutron-rich hypernuclei [14–19], the exploration of the hyperon drip line [20,21], as well as the feasibility of halo states in very light systems [22,23].

It is hence very interesting to investigate whether one or few Λ hyperons could also form halo structures in heavier Λ hypernuclei. In boron and carbon isotopes, the possibility of forming a halo structure has recently been investigated in the framework of the spherical Skyrme-Hartree-Fock (SHF) model [24]. Halo structures with wave functions extending beyond the nuclear surface were found in the Λ $1p$ states of light B and C isotopes. However, deformation and NN pairing, which both might have important effects on the halo structure, were not taken into consideration in Ref. [24].

Within a deformed SHF (DSHF) approach, the Λ hyperon has the possibility to occupy different $1p$ orbits, which leads to different shapes. For example, the Λ occupying the two orbits [101 1/2] and [101 3/2] can drive the nuclear core towards an oblate deformation, while occupying the orbit [110 1/2] favors a prolate shape [25,26]. Vice versa, also an eventual hyperon halo structure in the different Λ $1p$ orbits will be affected by core deformation and NN pairing.

Therefore, the main purpose of the present work is to investigate the interplay between deformation and change of the nuclear core and the hyperon halo structure in single- Λ p -shell hypernuclei. Note that such detailed modeling of hypernuclear structure will be required in the future for precise fitting of the ΛN interaction to weakly bound (halo) Λ states, which depend very sensitively on details of the nuclear core such as deformation and pairing. Accurate theoretical modeling is therefore necessary for comparison with experimental data on weakly bound Λ states. This has been

*xrzhou@phy.ecnu.edu.cn

recently demonstrated for the equivalent case of Ξ^- hypernuclei [27,28].

We will employ the axially deformed SHF model [29,30], which has been widely used to describe the gross characteristics of nuclei over a wide range of the nuclear chart. The Skyrme-type ΛN interaction proposed by Rayet in 1981 can describe well the hypernuclei in the Skyrme model [31]. Many Skyrme-type ΛN interactions have been postulated since then based on a large amount of hypernuclear data [20,32–37], and hypernuclear structure has been extensively studied employing these interactions [15,38,39]. For systematic calculations of hyperisotopes and comparison with Ref. [24], we will adopt the Skyrme-type ΛN interaction LY1 obtained by G -matrix calculations from a one-boson-exchange potential without ΛN spin-orbit (s.o.) force [34]. For discussing the dependence of the Λ removal energy on the ΛN interaction, we will also employ the global ΛN Skyrme interaction SLL4 [37,40], that fits very accurately the complete data set of currently known Λ hypernuclei.

The paper is organized as follows. In Sec. II, the formalism of the DSHF model and some numerical details are introduced. The results are presented in Sec. III, and a brief summary is given in Sec. IV.

II. FORMALISM

In the DSHF approach, the total energy of a hypernucleus is given by [16,20,31]

$$E = \int d^3\mathbf{r} \varepsilon(\mathbf{r}), \quad (1)$$

in which the energy functional is

$$\varepsilon = \varepsilon_N[\rho_n, \rho_p, \tau_n, \tau_p, \mathbf{J}_n, \mathbf{J}_p] + \varepsilon_\Lambda[\rho_n, \rho_p, \rho_\Lambda, \tau_\Lambda] \quad (2)$$

with ε_N and ε_Λ as contributions from NN and ΛN interactions, respectively. For the nucleonic energy-density functional ε_N , we use the standard Skyrme forces SIII [41], SGII [42], or SkI4 [43]. The energy-density functional due to the presence of hyperons, ε_Λ , reads [37]

$$\begin{aligned} \varepsilon_\Lambda = & \frac{\tau_\Lambda}{2m_\Lambda} + a_0\rho_\Lambda\rho_N + a_3\rho_\Lambda\rho_N^{1+\alpha} + a'_3\rho_\Lambda(\rho_N^2 + 2\rho_n\rho_p) \\ & + a_1(\rho_\Lambda\tau_n + \rho_n\tau_\Lambda) - a_2(\rho_\Lambda\Delta\rho_n + \rho_n\Delta\rho_\Lambda)/2 \\ & - a_4(\rho_\Lambda\nabla\cdot\mathbf{J}_n + \rho_n\nabla\cdot\mathbf{J}_\Lambda), \end{aligned} \quad (3)$$

where the last term is the s.o. part [24,37,38] and two alternative parametrizations of nonlinear effects are indicated, i.e., the first one a_3 derived from a G matrix [33,34,44] and the second one a'_3 from a YNN contact force [31,45]. The LY1 [34] and SLL4 [37,40] YN forces used in this work employ the first choice.

The one-body density ρ_q , kinetic density τ_q , and s.o. current \mathbf{J}_q read

$$[\rho_q, \tau_q, \mathbf{J}_q] = \sum_{k=1}^{N_q} n_q^k [|\phi_q^k|^2, |\nabla\phi_q^k|^2, \phi_q^{k*}(\nabla\phi_q^k \times \boldsymbol{\sigma})/i], \quad (4)$$

where ϕ_q^k ($k = 1, \dots, N_q$) are the single-particle (s.p.) wave functions of the k th occupied states for the different particles

$q = n, p, \Lambda$. The occupation probabilities n_q^k are calculated by taking into account pairing within a BCS approximation for nucleons only. The pairing interactions between nucleons are taken as a density-dependent δ force [46]:

$$V_q(\mathbf{r}_1, \mathbf{r}_2) = V'_q \left[1 - \frac{\rho_N((\mathbf{r}_1 + \mathbf{r}_2)/2)}{0.16 \text{ fm}^{-3}} \right] \delta(\mathbf{r}_1 - \mathbf{r}_2), \quad (5)$$

where pairing strengths $V'_p = V'_n = -410 \text{ MeV fm}^3$ are used for light nuclei [47]. A smooth energy cutoff is employed in the BCS calculations [48]. In the odd-mass systems, the orbit occupied by the unpaired nucleon is blocked as described in Ref. [49]. The unknown $\Lambda\Lambda$ pairing interaction is irrelevant for this work regarding only single- Λ hypernuclei.

Through the variation of the total energy (1) one derives the SHF Schrödinger equation for both nucleons and Λ hyperons,

$$\left[-\nabla \cdot \frac{1}{2m_q^*(\mathbf{r})} \nabla + V_q(\mathbf{r}) - i\mathbf{W}_q(\mathbf{r}) \cdot (\nabla \times \boldsymbol{\sigma}) \right] \phi_q^k(\mathbf{r}) = e_q^k \phi_q^k(\mathbf{r}), \quad (6)$$

in which $V_q(\mathbf{r})$ is the central part of the mean field depending on the densities, while $\mathbf{W}_q(\mathbf{r})$ is the s.o. interaction part [29]. The ΛN s.o. interaction is very small [24] and will be discussed later.

Each NN Skyrme force entails an approximate c.m. correction procedure that has been used for the parameter fitting. The SIII and SGII forces require to replace the bare masses in Eq. (6): $1/m_q \rightarrow 1/m_q - 1/M$, where $M = (N_n + N_p)m_N + N_\Lambda m_\Lambda$ is the total mass of the (hyper)nucleus. The SkI4 force uses an empirical correction $E_{\text{c.m.}} = -17.2 A^{-0.2} \text{ MeV}$. As the removal energy

$$B_\Lambda \equiv E(^A\text{Z}) - E(^{A+1}_\Lambda\text{Z}) \quad (7)$$

of Λ halo states can be arbitrarily small, the approximate character of the c.m. corrections (amongst other approximations for pairing, mean field, etc.) might represent a large relative theoretical error. For example, the difference between the above two procedures for C hyperisotopes is about 0.2 MeV. That is why we perform calculations with combinations of different NN and ΛN forces to ensure that our conclusions are qualitatively correct.

In the calculations, the DSHF Schrödinger equation is solved in cylindrical coordinates (r, z) , under the assumption of axial symmetry of the mean field [29,30]. The optimal quadrupole deformation parameters

$$\beta_2^{(q)} = \sqrt{\frac{\pi}{5}} \frac{\langle 2z^2 - r^2 \rangle_q}{\langle z^2 + r^2 \rangle_q} \quad (8)$$

are determined by minimizing the energy-density functional.

III. RESULTS AND DISCUSSION

In Ref. [24] the spherical SHF method has been applied to study the halo structure of the $\Lambda 1p$ state with the NN interaction SIII and the ΛN interaction LY1, which yields good predictions for the $\Lambda 1s$ binding energies of single- Λ hypernuclei. Here, we extend these calculations to deformed hypernuclei, evaluating different NN interactions SIII, SGII,

TABLE I. The lifetimes and dominant decay modes [electron capture (EC), β^- decay, or proton emission] of the nuclear cores. The data are taken from NuDat [50].

Nucleus	lifetime	dominant decay mode
^{10}C	19.3 s	EC
^{12}C	Stable	
^{14}C	5700 yr	β^-
^{16}C	0.747 s	β^-
^{18}C	92 ms	β^-
^{20}C	16.2 ms	β^-
^{22}C	6.1 ms	β^-
^9Li	178.3 ms	β^-
^{10}Be	$1.51 \times 10^{+6}$ yr	β^-
^{11}B	Stable	
^{13}N	598 s	EC
^{14}O	70.6 s	EC
^{15}F	10^{-15} s	p
^{16}Ne	9×10^{-21} s	2p

and SkI4, as well as ΛN interactions LY1 or SLL4. We perform systematic calculations for hyperisotopes with proton number $Z = 6$ and hyperisotones with neutron number $N = 6$.

The lifetimes and dominant decay modes of all the nuclear cores discussed in the article are listed in Table I. One can see that only ^{15}F and ^{16}Ne decay via the strong interaction by proton emission, whereas all others by weak decays (β decay and electron capture). Thus most of the nuclei discussed here are sufficiently long-lived to be experimentally relevant. Indeed several experiments to study neutron-rich or proton-rich hypernuclei are currently ongoing or planned [51–56]. Accurate total binding energies do exist in all cases and will be used in the following to compare with theoretical predictions of the various NN Skyrme forces.

The p -state hypernuclei built upon those nuclear cores are expected to decay electromagnetically, but it has also been conjectured [57] that the “nuclear Auger effect”, $^{A+1}_{\Lambda p}Z \rightarrow ^A_{\Lambda}Z + n$, might substantially broaden the Λ single-particle states to several 100 keV, although so far this effect has never been observed experimentally and the standard view of well-defined narrow hyperon single-particle states [58,59] seems to be well established. However, in particular for the Λ $1p$ states of neutron-rich nuclei discussed in this work, the relevance of the Auger effect might not be excluded and could in fact allow a detailed study of this phenomenon in the future. For the time being, the main interest of this work is in the Λ halo properties of hypernuclei and their interplay with a deformed core, assuming reasonably narrow Λ states.

A. Choice of interaction parameters

Figure 1 shows the total binding energies of the core nuclei ^{8-22}C obtained with the NN interactions SIII, SGII, and SkI4, respectively, in comparison with experimental data from Ref. [50]. One can see that SIII provides the best reproduction of the data, while SkI4 predicts a slight overbinding, which worsens for the SGII force. (This interaction was not optimized for fitting binding energies).

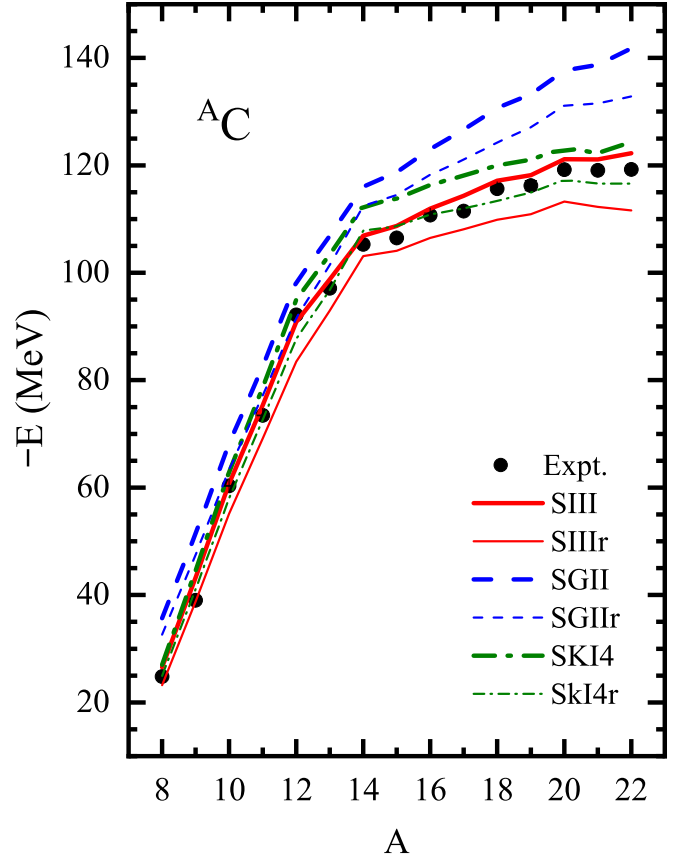


FIG. 1. Total binding energies of carbon isotopes with varying mass number A calculated with different Skyrme NN interactions SIII (solid red thick curve), SGII (dashed blue curve), and SkI4 (dash-dotted green curve), and with their modified variants SIIIr, SGIIr, and SkI4r (thin curves), in which the s.o. interaction is reduced to 60%. The experimental data [50] are also shown.

However, while the interaction SIII makes accurate predictions of total binding energies of C isotopes, it yields a spherical ground state for ^{12}C [15,25,65,66]. In Ref. [65] it was pointed out that the s.o. splitting of the s.p. levels around the Fermi surface plays an essential role for driving the nuclear deformation. Therefore, in order to obtain correctly deformed minima, the NN s.o. interactions are reduced to 60% of the original ones when calculating C (hyper)isotopes. The total binding energies calculated with these modified forces (labeled as “SIIIr”, “SGIIr”, and “SkI4r”) are also shown in Fig. 1. One can see that due to the reduced s.o. interaction, all binding energies are also reduced. Now SkI4r gives the best predictions for binding energies, while SIIIr provides slight underbinding, but SGIIr still overbinds most isotopes.

Next, these renormalized NN interactions are used in combination with the ΛN interactions LY1 or SLL4 to examine their predictions for the Λ $1s$ removal energy in C hyperisotopes. The results are shown in Fig. 2, together with available experimental data for $^{12,13,14}_{\Lambda}\text{C}$ from (π^+, K^+) [58], Emulsions1 [60], Emulsions2 [61], KEK-SKS [62], and DAΦNE-FINUDA [63,64].

One observes that results obtained with LY1 and SLL4 are both consistent with the data within the current error bars,

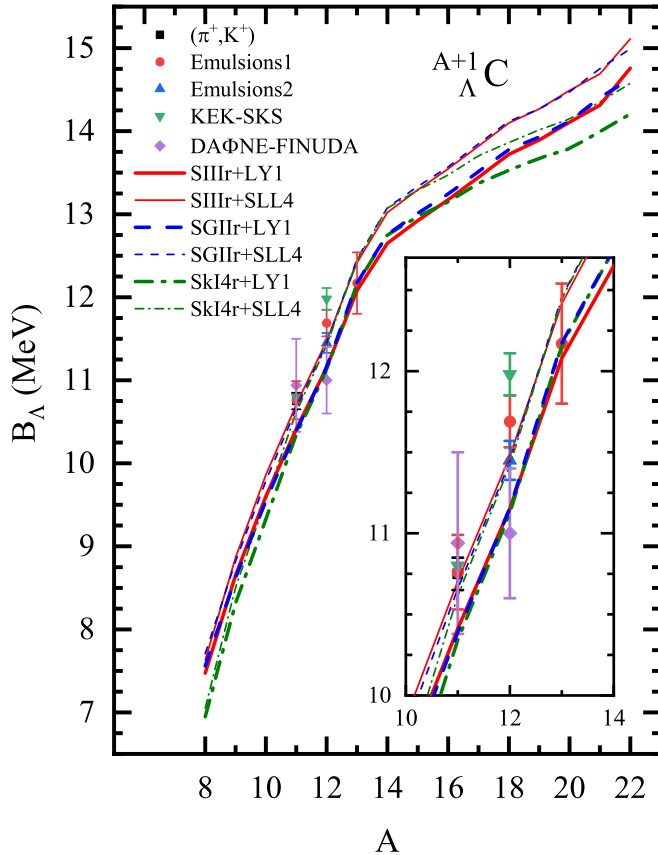


FIG. 2. Removal energies of the Λ $1s$ ground state of hypernuclei ${}^{A+1}_{\Lambda}\text{C}$ obtained with SIIIr, SGIIr, SkI4r, NN , and LY1 (thick curves) and SLL4 (thin curves) YN interactions, respectively. The experimental data (π^+ , K^+) [58], Emulsions1 [60], Emulsions2 [61], KEK-SKS [62], and DAΦNE-FINUDA [63,64] are also shown.

SLL4 providing about 0.3 MeV more binding. Furthermore, B_{Λ} is almost independent of the NN interaction for $12 \leq A \leq 18$, while in the proton-rich and neutron-rich regions SkI4r predicts up to about 0.5 MeV less binding than SIIIr or SGIIr. Therefore we will use SIIIr+LY1 as the default interaction in the following analysis.

B. Deformations of carbon hyperisotopes

In Fig. 3, the potential energy surfaces of core nuclei ${}^A\text{C}$ and Λ $1p$ hypernuclei ${}^{A+1}_{\Lambda}\text{C}$ obtained by self-consistent DSHF calculations with SIIIr+LY1, SGIIr+LY1, and SkI4r+LY1 interactions are compared. For hypernuclei, the results with the Λ in $[101\ 1/2]$ and $[110\ 1/2]$ orbits are given. All interactions predict energy minima of the normal nuclei and hypernuclei on the same deformation side. The energy minima of ${}^{10}\text{C}$ and ${}^{12}\text{C}$ are oblate with $\beta_2 \approx -0.32$. ${}^{14}\text{C}$ is a spherical nucleus because of the neutron $N = 8$ closed-shell effect. The energy minimum of ${}^{16}\text{C}$ is on the prolate side. Two minima with almost the same energies appear on the prolate and oblate sides for ${}^{18}\text{C}$, and the deformation becomes oblate again for ${}^{20}\text{C}$ and ${}^{22}\text{C}$. The corresponding values of total energy E , removal energy B_{Λ} , as well as the deformations of the

hypernuclei β_2 and the Λ hyperon density $\beta_2^{(\Lambda)}$ are summarized in Table II.

As already evident in Figs. 1 and 2, one notes that there is a quite big difference between SIIIr+LY1, SGIIr+LY1, and SkI4r+LY1 results for the total energies of the (hyper)nuclei, whereas the Λ $1p$ removal energies are almost independent of the NN interaction, in line with the spherical SHF results [24]. Since we mainly focus on the effect of deformation on hyperon halo structure, the good description of the hypernuclear deformation and the robust prediction of the Λ removal energy provide a reliable environment to investigate the Λ halo structure in the following.

C. Interplay between deformation and hyperon halos

We now discuss the differences between the spherical and axially deformed systems with a Λ $1p$ state. For this purpose, quadrupole-constrained calculations were carried out in the DSHF to obtain results with spherical shape. To guarantee that the deformations of hypernuclei, cores, and hyperons are all constrained to be spherical, the three Λ $1p$ orbits $[101\ 1/2]$, $[101\ 3/2]$, and $[110\ 1/2]$ should be mixed with the same occupation probability (labeled as “spherical”). The obtained energies E and the induced Λ removal energies B_{Λ} are also given in Table II. One again observes that the three interactions give similar results for $\beta_2^{(\Lambda)}$.

For ${}^{11}_{\Lambda}\text{C}$, the Λ $1p$ states except $[110\ 1/2]$ are unbound with respect to the ${}^{10}\text{C} + \Lambda$ threshold, since their removal energies B_{Λ} are negative. The Λ $[110\ 1/2]$ state has a prolate shape and thus tends to move the core deformation to the prolate side, as can clearly be seen in Fig. 3. The deformations of ${}^{11}_{\Lambda}\text{C}$ and Λ are 0.47/0.48/0.46 and 0.77/0.78/0.77 with SIIIr/SGIIr/SkI4r forces, respectively. Because B_{Λ} of the $[110\ 1/2]$ state is only slightly larger than the typical weak binding energy 1 MeV [3], ${}^{11}_{\Lambda}\text{C}$ possibly has a prolately deformed halo structure in this state, which the spherical SHF calculation in Ref. [24] could not evidence.

For ${}^{13}_{\Lambda}\text{C}$, almost all Λ $1p$ states, except $[110\ 1/2]$ with SkI4r+LY1, are bound with respect to the ${}^{12}\text{C} + \Lambda$ threshold. The removal energy of the spherical state is substantially less than those of the two deformed states $[101\ 1/2]$ and $[110\ 1/2]$, indicating that deformation has a considerable influence on the bound state of hypernuclei. B_{Λ} values of both spherical and prolate $[110\ 1/2]$ states are smaller than the typical weak binding energy 1 MeV, indicating a possible halo structure in both cases. However, the true ground state is the oblate $[101\ 1/2]$ and this thus counteracts the formation of a Λ $[110\ 1/2]$ halo. In fact B_{Λ} of the prolately deformed ${}^{15}_{\Lambda}\text{C}$ is of the same size as for the oblate ${}^{13}_{\Lambda}\text{C}$. For ${}^{17}_{\Lambda}\text{C}$ and heavier isotopes the Λ is always stronger bound and no further halos appear.

Since the various weakly bound Λ $1p$ states depend very delicately on the interactions employed, we study this in more detail in Table III, which lists also results obtained with the SLL4 ΛN force for comparison. The differences between LY1 and SLL4 results are generally very small. In nearly all cases the deformed states are more bound than the spherical states. However, the theoretical B_{Λ} values differ by the order of 1 MeV in the differently deformed states, which is important for future precise fits of the ΛN interaction. For

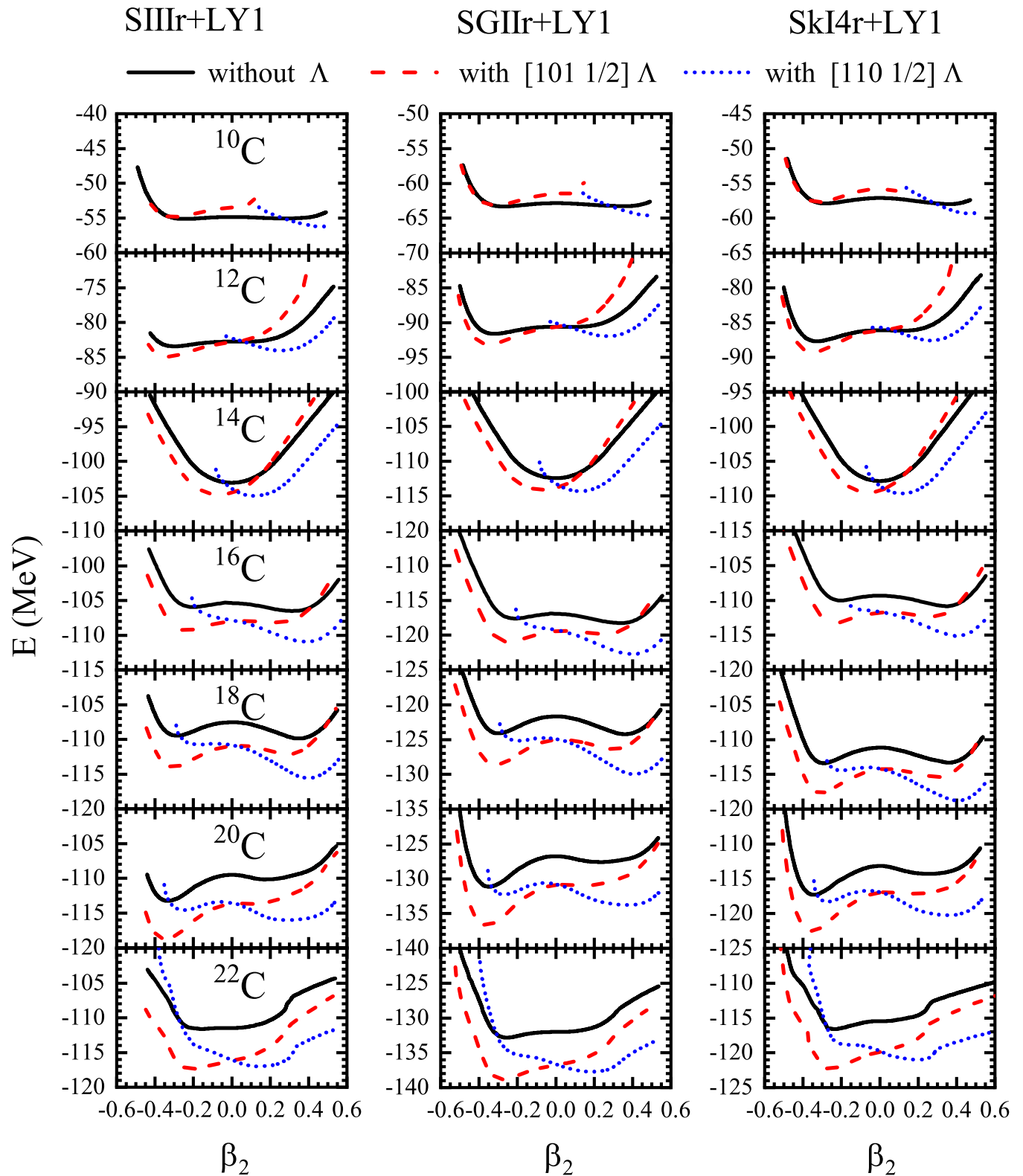


FIG. 3. Potential energy surfaces of C (hyper)isotopes obtained by self-consistent DSHF calculations with SIIIr/SGIIr/SkI4r+LY1 interactions. The solid curves represent the potential energy surface of nuclei without Λ and the dashed and dotted curves hypernuclei with Λ $[101\ 1/2]$ and $[110\ 1/2]$ p states, respectively.

TABLE II. Deformations β_2 and $\beta_2^{(\Lambda)}$ of hypernucleus and Λ hyperon individually, total energies E (in MeV), and Λ removal energies B_Λ (in MeV) of C hyperisotopes with different Λ $1p$ states calculated by DSHF using SIIIr/SGIIr/SkI4r+LY1 interactions. For spherical results the three Λ $1p$ orbits [101 1/2], [101 3/2], and [110 1/2] are mixed with the same occupation probability in the calculations. The ‘*’ indicates the deformed state with minimum energy.

hypernucleus	deformed								spherical		
	[101 1/2]				[110 1/2]				mixed		
	β_2	$\beta_2^{(\Lambda)}$	$-E$	B_Λ	β_2	$\beta_2^{(\Lambda)}$	$-E$	B_Λ	$-E$	B_Λ	
SIIIr+LY1	$^{11}_\Lambda\text{C}$	-0.30	-0.37	54.9	-0.27	0.47	0.77	56.2*	1.10	53.7	-1.14
	$^{13}_\Lambda\text{C}$	-0.34	-0.40	84.9*	1.49	0.26	0.70	84.1	0.62	83.0	0.25
	$^{15}_\Lambda\text{C}$	-0.07	-0.33	104.8	1.70	0.13	0.66	105.0*	1.89	104.7	1.63
	$^{17}_\Lambda\text{C}$	-0.24	-0.38	109.3	2.79	0.39	0.79	110.9*	4.43	108.1	2.75
	$^{19}_\Lambda\text{C}$	-0.31	-0.41	114.0	4.08	0.40	0.78	115.6*	5.68	111.0	3.46
	$^{21}_\Lambda\text{C}$	-0.34	-0.43	118.7*	5.46	0.29	0.75	116.0	2.75	113.7	4.20
	$^{23}_\Lambda\text{C}$	-0.22	-0.40	117.3*	5.72	0.14	0.70	117.0	5.39	116.3	4.79
SGIIr+LY1	$^{11}_\Lambda\text{C}$	-0.32	-0.38	63.1	-0.20	0.48	0.78	64.6*	1.28	61.7	-1.15
	$^{13}_\Lambda\text{C}$	-0.35	-0.40	93.1*	1.53	0.27	0.71	92.0	0.34	90.8	0.19
	$^{15}_\Lambda\text{C}$	-0.07	-0.33	114.1	1.66	0.13	0.66	114.3*	1.87	114.0	1.57
	$^{17}_\Lambda\text{C}$	-0.24	-0.38	121.0	2.71	0.40	0.79	122.7*	4.47	119.5	2.55
	$^{19}_\Lambda\text{C}$	-0.32	-0.42	128.6	4.39	0.41	0.79	130.0*	5.73	125.1	3.42
	$^{21}_\Lambda\text{C}$	-0.36	-0.44	136.6*	5.50	0.37	0.37	133.7	2.60	130.9	4.18
	$^{23}_\Lambda\text{C}$	-0.28	-0.41	138.8*	5.99	0.19	0.71	137.7	4.90	136.8	4.80
SkI4r+LY1	$^{11}_\Lambda\text{C}$	-0.32	-0.38	57.7	-0.30	0.46	0.77	59.3*	1.34	56.0	-1.15
	$^{13}_\Lambda\text{C}$	-0.35	-0.40	89.2*	1.54	0.27	0.71	87.6	-0.13	86.3	0.19
	$^{15}_\Lambda\text{C}$	-0.06	-0.33	109.5	1.62	0.11	0.65	109.7*	1.79	109.4	1.56
	$^{17}_\Lambda\text{C}$	-0.23	-0.38	113.2	2.37	0.40	0.78	115.1*	4.28	111.8	2.48
	$^{19}_\Lambda\text{C}$	-0.31	-0.41	117.7	4.25	0.41	0.78	118.8*	5.38	114.3	3.15
	$^{21}_\Lambda\text{C}$	-0.35	-0.43	122.5*	5.22	0.36	0.77	120.2	2.94	117.0	3.84
	$^{23}_\Lambda\text{C}$	-0.26	-0.41	122.3*	5.66	0.20	0.73	121.0	4.37	119.9	4.47

example, both LY1 and SLL4 parameters (and actually all current ΛN Skyrme forces) were obtained from theoretical calculations without taking into account deformation, and this is one of the issues to be addressed in the future for more precise parameter fits. As it stands, for both SLL4 and LY1 the B_Λ of the deformed states agree better than those of the spherical state with the known experimental data for $^{13}_\Lambda\text{C}$.

We also verify in Table III (last two ‘Theory’ columns) that the removal energies of Λ spherical states computed with the unrenormalized SIII+LY1 force are very close to the equivalent ones of Ref. [24], and that the difference to the SIIIr+LY1 results is very small.

To illustrate the mechanism that lowers the p -state energies in the differently deformed states, we plot in Fig. 4 the Λ mean field V_Λ (upper panels) and the density distribution ρ_Λ (lower panels) in the spherical and deformed hypernuclei $^{11,13}_\Lambda\text{C}$. One sees that for the prolately deformed $^{11}_\Lambda\text{C}$, which contains a Λ [110 1/2] state, the potential well in the $r = 0$ plane (thick dotted blue curve) is deeper by several MeV in the region around $z \approx 2.0$ fm, where a major part of the prolate [110 1/2] wave function resides. This leads to an energy gain of the

lent ones of Ref. [24], and that the difference to the SIIIr+LY1 results is very small.

TABLE III. Λ removal energies B_Λ (in MeV) of C hyperisotopes with different Λ $1p$ states calculated by DSHF with different $NN+\Lambda N$ interactions. Experimental data are also shown.

	Theory									Experiment	
	[101 1/2]		[110 1/2]		Spherical			Ref. [24]	Ref. [59]		
	SIIIr+SLL4	SIIIr+LY1	SIIIr+SLL4	SIIIr+LY1	SIIIr+SLL4	SIII+SLL4	SIIIr+LY1	SIII+LY1	SIII+LY1	(π^+, K^+)	Emulsion
$^{11}_\Lambda\text{C}$	-0.50	-0.27	1.01	1.10	-1.42	-1.50	-1.14	-1.23	-	-	-
$^{13}_\Lambda\text{C}$	1.37	1.49	0.48	0.62	0.00	-0.08	0.25	0.18	0.19	1.1(2)	0.8(3)
$^{15}_\Lambda\text{C}$	1.53	1.70	1.75	1.89	1.45	1.41	1.63	1.60	1.61	-	-
$^{17}_\Lambda\text{C}$	2.69	2.79	4.41	4.43	2.59	2.43	2.75	2.60	2.58	-	-
$^{19}_\Lambda\text{C}$	4.03	4.08	5.71	5.68	3.31	3.35	3.46	3.51	3.50	-	-
$^{21}_\Lambda\text{C}$	5.45	5.46	2.77	2.75	4.07	4.24	4.20	4.37	4.38	-	-
$^{23}_\Lambda\text{C}$	5.70	5.72	5.35	5.39	4.65	4.71	4.79	4.87	4.88	-	-

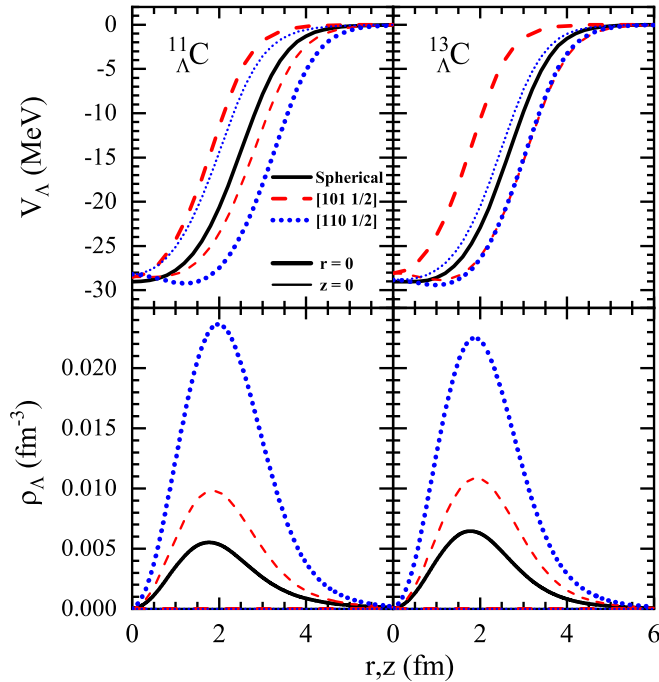


FIG. 4. The Λ mean field V_Λ (upper panels) and density distribution ρ_Λ (lower panels) in the spherical and deformed hypernuclei $^{11,13}_\Lambda\text{C}$, obtained with SIIIr+LY1 forces. The results for $r = 0$ (thick curves) and $z = 0$ (thin curves) of the Λ [101 1/2] state (dashed red curves) and the Λ [110 1/2] state (dotted blue curves) are shown. The solid black curves show the results of the spherical calculation.

order of 1 MeV for the binding of the Λ compared to the [101 1/2] state. Similarly, the potential well of the [101 1/2] state in the $z = 0$ plane (thin dashed red curve) causes an energy gain of about 1 MeV compared to the spherical state (solid black curve). This explains the B_Λ values listed in Table II.

For the oblatelly deformed $^{13}_\Lambda\text{C}$, the potential wells in the $r = 0/z = 0$ plane of the [110 1/2]/[101 1/2] states are very similar in the region of maximum prolate/oblate wave functions. As discussed in detail in Ref. [27], oblate deformation of the nuclear core ^{12}C favors the binding of an oblate Λ $1p$ orbital, because of the improved geometrical overlap of wave function and embedding potential, such that this state becomes more bound than in spherical approximation or prolate deformation.

The prolate and oblate energy minima of $^{15,17,19}_\Lambda\text{C}$ and $^{21,23}_\Lambda\text{C}$, respectively, are explained in the same manner. Altogether, it can be stated that the depth of the hyperon potential and the geometrical overlap of the wave function of hyperon and the nuclear core play roles in the binding of hypernuclei, and that the two mechanisms may compete.

D. Effects of core on hyperon halo

In order to investigate now the effect of deformation on the hyperon halo structure in more detail, density contours of different Λ $1p$ states are drawn in Fig. 5. The densities of the Λ [101 1/2] ([110 1/2]) states are symmetric in the r (z) direction. We find results in line with the B_Λ values in Table II, namely weakly bound states extend further out than strongly

bound ones, in particular the spherical and [110 1/2] states extend up to about 15 fm (using $\rho = 10^{-8} \text{ fm}^{-3}$ as a density threshold) for the $^{11,13,15}_\Lambda\text{C}$ isotopes, which is beyond the core nucleus densities plotted in the last column for comparison, whereas for heavier isotopes the Λ is fully embedded in the core.

In fact the corresponding one-dimensional density distributions plotted in Fig. 6 show that the Λ density for $^{11,13,15}_\Lambda\text{C}$ exceeds the neutron density by about two orders of magnitude at $r \approx 10$ fm, for all types of deformation, and thus constitutes a proper Λ ‘halo’, even for $^{15}_\Lambda\text{C}$ with $B_\Lambda \gtrsim 1$ MeV. On the contrary, in $^{17}_\Lambda\text{C}$ and heavier isotopes the Λ density behaves as the neutron density and a Λ halo is not present any more (or merges with the neutron halo).

These features are also confirmed by the root-mean-square (rms) radii of protons, neutrons, and Λ that are indicated by arrows in Fig. 6. One sees that larger B_Λ causes smaller Λ radii, also consistent with the results of spherical SHF in Ref. [24]. In particular, the Λ radii in spherical states are larger than those in deformed states due to the weaker binding. Comparing with the density contours in Fig. 5, the greater geometrical weight in r direction should be taken into account, and therefore an extended halo in z direction ([110 1/2] state) might not be adequately reflected by the rms radius, see, e.g., $^{11,13}_\Lambda\text{C}$. In any case, for the light isotopes the Λ radii are always substantially larger than the nucleonic ones, confirming the Λ halo structure.

Thus, different Λ $1p$ orbits drive hypernuclei towards different deformations and thereby affect the density distribution of the Λ as well as their halo structure. The results obtained for light C hyperisotopes have shown that hyperons occupying $1p$ orbits may be in weakly bound states and diffuse in space with very small density and thus form hyperon halos. With increasing mass number the Λ becomes more bound and the halo disappears. We therefore study in Table IV and Fig. 7 the same effect in $N = 6$ hyperisotones (with the common nucleus $^{13}_\Lambda\text{C}$) with the SIIIr+LY1 interaction. Due to the isoscalar ΔN interaction, the effects found here are very similar to those for the hyperisotopes: up to a mass number $A \approx 15$, the hyperon is unbound or forms a halo state with large rms radius r_Λ , in particular for the [101 1/2] orbit. For these light nuclei, the Λ occupies a halo outside the nuclear core, as seen in Fig. 7, while with increasing mass number it is gradually absorbed into the nuclear core. $^{17}_\Lambda\text{Ne}$ does not exhibit a halo anymore, just like $^{17}_\Lambda\text{C}$ before. Equivalent results were obtained in spherical SHF [24].

As for C hyperisotopes, the Λ [101 1/2]/[110 1/2] state has oblate/prolate shape and thus tends to move the core deformation to the oblate/prolate side, by the mechanism that lowers the p -state energies in the differently deformed states discussed with Fig. 4. The theoretical B_Λ values are different in the oblate and prolate states by up to about 2 MeV. Almost all energy minima of $N = 6$ hyperisotones are on the prolate side, only $^{13}_\Lambda\text{C}$ is oblate. Regarding $^{14}_\Lambda\text{N}$ and $^{15}_\Lambda\text{O}$, because of the spherical core shape and the proton closed-shell effect, the depth of the Λ [101 1/2] and [110 1/2] potential wells and the related removal energies are very similar.

Concerning experimental data, although the ground-state Λ removal energy of $^{14}_\Lambda\text{N}$ has not been observed, it might

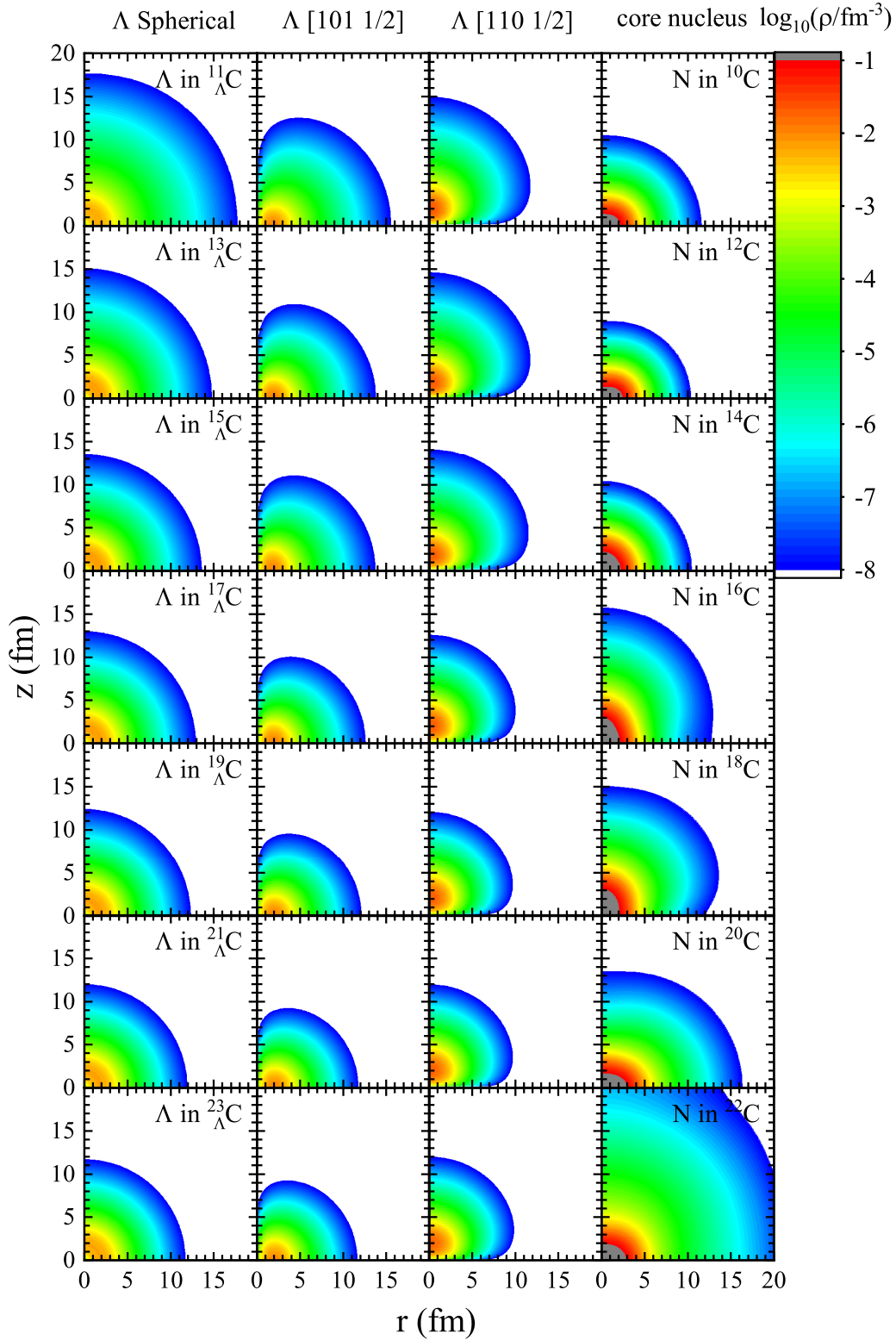


FIG. 5. The density distributions of spherical and deformed $[101\ 1/2]$ and $[110\ 1/2]$ Λ $1p$ states in C hyperisotopes compared to the nuclear density distributions in the core nuclei, calculated by DSHF with the SIIIr+LY1 interaction. In the spherical calculations, the three Λ $1p$ orbits $[101\ 1/2]$, $[101\ 3/2]$, and $[110\ 1/2]$ are mixed with the same occupation probabilities. Neutrons in the core nucleus ^{22}C are unbound.

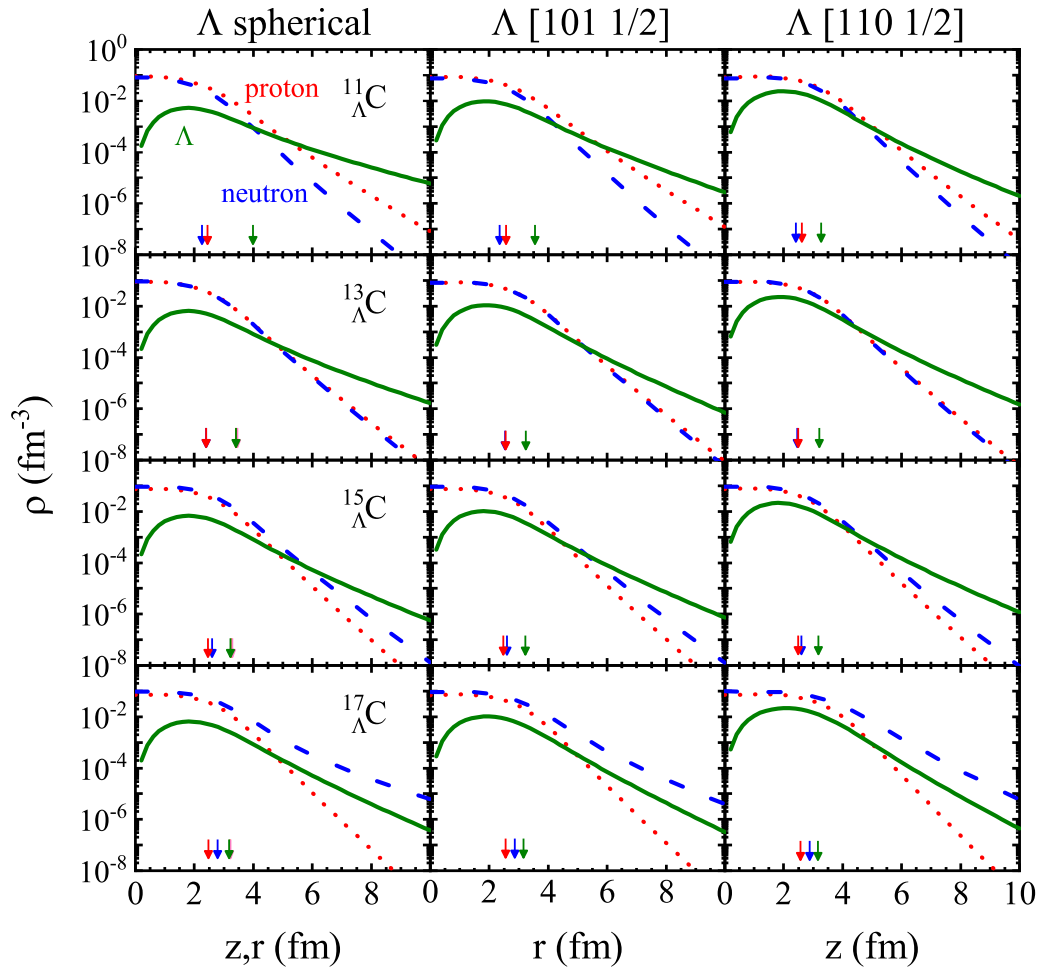


FIG. 6. The density distributions of spherical and deformed Λ $1p$ states in C hyperisotopes compared to the density distributions of neutron and proton, calculated by DSHF with the SIIIr+LY1 interaction. Arrows indicate the rms radii.

be approximated by the one for the mirror nucleus $^{14}_{\Lambda}\text{C}$, $B_{\Lambda_s} = 12.17 \pm 0.33$ MeV [60]. Making this assumption, in Ref. [67] the difference between the Λ $1s$ and $1p$ states for $^{14}_{\Lambda}\text{N}$ was determined to be about 10.5 MeV. The resulting $B_{\Lambda_p} \approx 1.67$ MeV compares fairly well with our theoretical values in Table IV.

E. ΛN spin-orbit splitting in $^{13}_{\Lambda}\text{C}$

The Λ $1p$ halo states discussed in the previous sections are weakly bound by less than 1 MeV, which is comparable to the finer effects of the ΛN interaction, such as the s.o. splitting, for which experimental data are available for the $^{13}_{\Lambda}\text{C}$ hypernucleus. The dominant component of the two negative-

TABLE IV. Λ removal energies (in MeV), rms radii (in fm), and deformations of $N = 6$ hyperisotones for the Λ [101 1/2] and [110 1/2] states calculated by DSHF using the SIIIr+LY1 interaction. The ‘*’ indicates the deformed state with minimum energy. The $^{17}_{\Lambda}\text{Ne}$ core nucleus is unbound.

	core nucleus			[101 1/2]			[110 1/2]		
	$-E$	r_N	β_2	B_{Λ}	r_{Λ}	β_2	B_{Λ}	r_{Λ}	β_2
$^{10}_{\Lambda}\text{Li}$	44.70	2.44	-0.20	-1.24	4.03	-0.26	-0.24*	3.52	0.38
$^{11}_{\Lambda}\text{Be}$	59.56	2.44	-0.23	-0.30	3.54	-0.30	1.02*	3.26	0.47
$^{12}_{\Lambda}\text{B}$	71.61	2.48	-0.28	0.64	3.35	-0.33	0.92*	3.23	0.35
$^{13}_{\Lambda}\text{C}$	83.44	2.53	-0.32	1.49*	3.25	-0.34	0.62	3.21	0.26
$^{14}_{\Lambda}\text{N}$	90.10	2.51	0	1.31	3.23	-0.19	1.50*	3.20	0.17
$^{15}_{\Lambda}\text{O}$	97.05	2.57	0	1.69	3.23	-0.06	1.88*	3.18	0.13
$^{16}_{\Lambda}\text{F}$	94.84	2.74	0.21	1.67	3.23	-0.12	3.23*	3.15	0.27
$^{17}_{\Lambda}\text{Ne}$	93.65	2.85	0.34	2.45	3.17	-0.25	4.35*	3.19	0.41

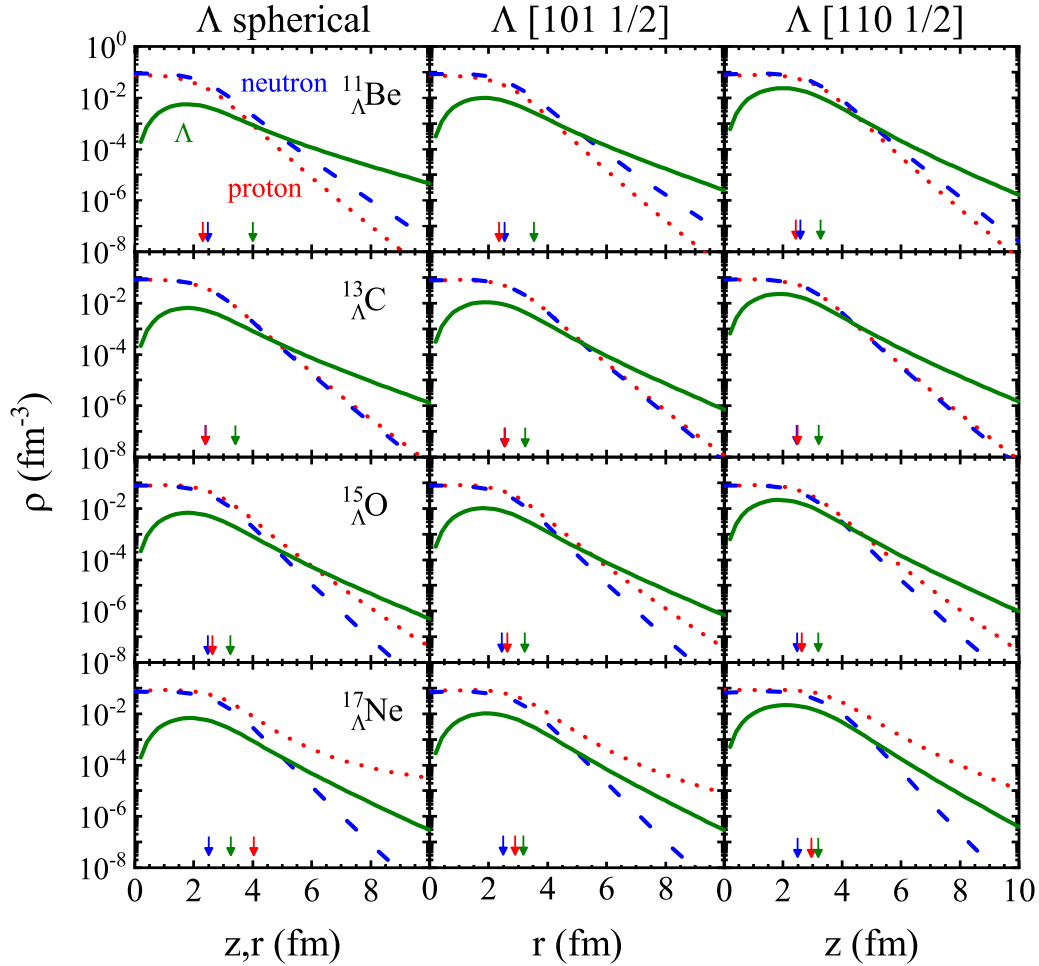


FIG. 7. Same as Fig. 6, but for $N = 6$ hyperisotopes. A proton in spherical $^{17}_{\Lambda}\text{Ne}$ is unbound.

parity states $1/2^-$ and $3/2^-$ in $^{13}_{\Lambda}\text{C}$ is the $^{12}\text{C}_{\text{g.s.}}(0^+) \otimes \Lambda_{1p}$ configuration. In Refs. [68,69] the s.o. splitting was measured as $E(1/2^-) - E(3/2^-) = 0.152 \pm 0.054(\text{stat}) \pm 0.036(\text{syst})$ MeV in the reaction $^{13}\text{C}(K^-, \pi^- \gamma)^{13}_{\Lambda}\text{C}$ via the substitutional transition $(p_{1/2})_n \rightarrow (p_{3/2})_{\Lambda}$ on the ordinary oblatelly deformed core nucleus ^{13}C . The excitation energies of the $1/2^-$ and $3/2^-$ states were determined as 10.98 and 10.83 MeV, respectively, by analyzing the different angular distributions of the reaction for the two channels.

In the spherical SHF calculation [24], these experimental data correspond to the $\Lambda 1p_{1/2}$ and $1p_{3/2}$ states and they were reproduced with a s.o. force strength $a_4 = W_0^{\Lambda}/2 = 2.35$ MeV fm⁵ in Eq. (3). As the initial ^{13}C core nucleus is oblatelly deformed, in our two-dimensional model they correspond thus to the oblatelly deformed Λ states $[101 1/2]$ and $[101 3/2]$, which are degenerate without an additional Λ s.o. force ($a_4 = 0$). In this work with the SIIIr+LY1/SLL4 interactions, the splitting of the $[101 1/2]$ and $[101 3/2]$ states may be adjusted to the experimental data of $^{13}_{\Lambda}\text{C}$ with a value $a_4 = W_0^{\Lambda}/2 = 2.65$ MeV fm⁵, as is illustrated in Fig. 8, with the corresponding excitation energies $E_{1/2} = 9.84(10.29)$ MeV and $E_{3/2} = 9.69(10.14)$ MeV for the SIIIr+LY1(SLL4) interaction.

Instead, the prolate $[110 1/2]$ state remains at a higher energy. It would be very difficult to observe this state experimentally, as it requires a collective configuration change from the oblate true ^{13}C ground state to the excited prolate one, which is supposedly very short-lived. Also, theoretically a beyond-mean-field approach [70–72] would be appropriate for a more realistic modeling of this phenomenon.

These results confirm that the combined treatment of deformation and details of the ΛN interaction such as a s.o. force is necessary for a precise fitting and understanding of experimental data, as motivated in the Introduction.

In this regard, the small ΛN spin-orbit force also provides small additional binding for the $\Lambda 1s$ orbits, of about 0.1 MeV for the C hyperisotopes. However, this is a spurious effect, as the parameters of both LY1 and SLL4 forces were determined with $a_4 = 0$, and would have to be refitted when including the s.o. force (and other improvements of the formalism such as deformation discussed here).

IV. SUMMARY

The mutual interplay between nuclear core deformation and hyperon halo structure in single- Λ p -shell C hyperisotopes and $N = 6$ hyperisotopes has been studied in the

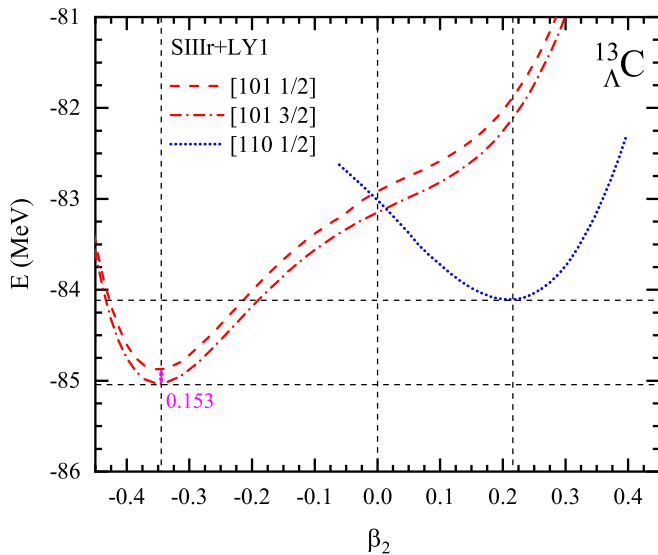


FIG. 8. Self-consistent DSHF results of different Λ $1p$ states in $^{13}_{\Lambda}\text{C}$ using the SIIIr+LY1 interaction with $a_4 = 2.65 \text{ MeV fm}^5$.

DSHF framework with the interactions SIIIr/SGIr/Ski4r + LY1/SLL4. We found Λ halo states characterized by weak Λ binding $\lesssim 1 \text{ MeV}$ and extended density distributions up to mass number $A = 15$. With the increase of the nucleon

number the halo state gradually disappears, until the Λ is absorbed completely into the nuclear core.

Generally deformation causes more deeply bound Λ states with smaller diffusion of the density distributions and related radii. In any case the difference between Λ removal energies in the differently deformed states is of the order of 1 MeV, depending somewhat on the choice of the interactions. This is comparable to the magnitude of the ΛN s.o. splitting, for example.

Therefore these kind of results will be important for future precise fits of the ΛN interaction, in particular for weakly bound Λ s.p. states, where deformation is important and has to be necessarily considered for precise calculations of the Λ removal energies to be compared with experimental values. This work is a first step in that direction. In particular, a beyond-mean-field treatment [70–72] and inclusion of the decay widths might also be required for a more realistic modeling in the future.

ACKNOWLEDGMENTS

Helpful discussions with Prof. H. Sagawa are gratefully acknowledged. This work was supported by the National Natural Science Foundation of China under Grants No. 12175071, No. 11775081, and No. 11875134, and the National Natural Science Foundation for Young Scientists of China under Grant No. 12205103.

- [1] I. Tanihata, H. Hamagaki, O. Hashimoto, Y. Shida, N. Yoshikawa, K. Sugimoto, O. Yamakawa, T. Kobayashi, and N. Takahashi, *Phys. Rev. Lett.* **55**, 2676 (1985).
- [2] B. Jonson, *Phys. Rep.* **389**, 1 (2004).
- [3] A. S. Jensen, K. Riisager, D. V. Fedorov, and E. Garrido, *Rev. Mod. Phys.* **76**, 215 (2004).
- [4] J. Meng and S. G. Zhou, *J. Phys. G* **42**, 093101 (2015).
- [5] T. Nakamura *et al.*, *Phys. Rev. Lett.* **96**, 252502 (2006).
- [6] N. Kobayashi *et al.*, *Phys. Rev. Lett.* **112**, 242501 (2014).
- [7] P. G. Hansen and B. Jonson, *Europhys. Lett.* **4**, 409 (1987).
- [8] T. Nakamura *et al.*, *Phys. Rev. Lett.* **103**, 262501 (2009).
- [9] M. Takechi *et al.*, *Phys. Lett. B* **707**, 357 (2012).
- [10] T. Nakamura *et al.*, *Phys. Rev. Lett.* **112**, 142501 (2014).
- [11] J. Meng and P. Ring, *Phys. Rev. Lett.* **80**, 460 (1998).
- [12] Y. Zhang, M. Matsuo, and J. Meng, *Phys. Rev. C* **86**, 054318 (2012).
- [13] M. Danysz and J. Pniewski, *Philos. Mag. J. Sci.* **44**, 348 (1953).
- [14] D. Vretenar, W. Pöschl, G. A. Lalazissis, and P. Ring, *Phys. Rev. C* **57**, R1060(R) (1998).
- [15] X.-R. Zhou, H.-J. Schulze, H. Sagawa, C.-X. Wu, and E.-G. Zhao, *Phys. Rev. C* **76**, 034312 (2007).
- [16] X.-R. Zhou, A. Polls, H.-J. Schulze, and I. Vidaña, *Phys. Rev. C* **78**, 054306 (2008).
- [17] A. Umeya and T. Harada, *Phys. Rev. C* **79**, 024315 (2009).
- [18] A. Gal and D. Millener, *Phys. Lett. B* **725**, 445 (2013).
- [19] R. Wirth and R. Roth, *Phys. Lett. B* **779**, 336 (2018).
- [20] J. Cugnon, A. Lejeune, and H.-J. Schulze, *Phys. Rev. C* **62**, 064308 (2000).
- [21] E. Khan, J. Margueron, F. Gulminelli, and A. R. Raduta, *Phys. Rev. C* **92**, 044313 (2015).
- [22] K. Miyagawa, H. Kamada, W. Glöckle, and V. Stoks, *Phys. Rev. C* **51**, 2905 (1995).
- [23] E. Hiyama, M. Kamimura, T. Motoba, T. Yamada, and Y. Yamamoto, *Phys. Rev. C* **53**, 2075 (1996).
- [24] Y. Zhang, H. Sagawa, and E. Hiyama, *Phys. Rev. C* **103**, 034321 (2021).
- [25] B.-C. Fang, W.-Y. Li, C.-F. Chen, J.-W. Cui, X.-R. Zhou, and Y.-Y. Cheng, *Eur. Phys. J. A* **56**, 11 (2020).
- [26] C. F. Chen, Q. B. Chen, X.-R. Zhou, Y. Y. Cheng, J.-W. Cui, and H.-J. Schulze, *Chin. Phys. C* **46**, 064109 (2022).
- [27] Y. Jin, X.-R. Zhou, Y.-Y. Cheng, and H.-J. Schulze, *Eur. Phys. J. A* **56**, 135 (2020).
- [28] J. Guo, X.-R. Zhou, and H.-J. Schulze, *Phys. Rev. C* **104**, L061307 (2021).
- [29] D. Vautherin, *Phys. Rev. C* **7**, 296 (1973).
- [30] M. Bender, P.-H. Heenen, and P.-G. Reinhard, *Rev. Mod. Phys.* **75**, 121 (2003).
- [31] M. Rayet, *Nucl. Phys. A* **367**, 381 (1981).
- [32] Y. Yamamoto, H. Bandō, and J. Žofka, *Prog. Theor. Phys.* **80**, 757 (1988).
- [33] D. J. Millener, C. B. Dover, and A. Gal, *Phys. Rev. C* **38**, 2700 (1988).
- [34] D. E. Lansky and Y. Yamamoto, *Phys. Rev. C* **55**, 2330 (1997).
- [35] I. Vidaña, A. Polls, A. Ramos, and H.-J. Schulze, *Phys. Rev. C* **64**, 044301 (2001).
- [36] H.-J. Schulze and T. Rijken, *Phys. Rev. C* **88**, 024322 (2013).
- [37] H.-J. Schulze and E. Hiyama, *Phys. Rev. C* **90**, 047301 (2014).
- [38] M. T. Win, K. Hagino, and T. Koike, *Phys. Rev. C* **83**, 014301 (2011).

- [39] A. Li, E. Hiyama, X.-R. Zhou, and H. Sagawa, *Phys. Rev. C* **87**, 014333 (2013).
- [40] H.-J. Schulze, *AIP Conf. Proc.* **2130**, 020009 (2019).
- [41] M. Beiner, H. Flocard, N. Van Giai, and P. Quentin, *Nucl. Phys. A* **238**, 29 (1975).
- [42] N. Van Giai and H. Sagawa, *Nucl. Phys. A* **371**, 1 (1981).
- [43] P.-G. Reinhard and H. Flocard, *Nucl. Phys. A* **584**, 467 (1995).
- [44] N. Guleria, S. K. Dhiman, and R. Shyam, *Nucl. Phys. A* **886**, 71 (2012).
- [45] M. Rayet, *Ann. Phys.* **102**, 226 (1976).
- [46] N. Tajima, P. Bonche, H. Flocard, P.-H. Heenen, and M. Weiss, *Nucl. Phys. A* **551**, 434 (1993).
- [47] T. Suzuki, H. Sagawa, and K. Hagino, *Phys. Rev. C* **68**, 014317 (2003).
- [48] M. Bender, K. Rutz, P.-G. Reinhard, and J. Maruhn, *Eur. Phys. J. A* **8**, 59 (2000).
- [49] P. Ring and P. Schuck, *The Nuclear Many-Body Problem* (Springer Science & Business Media, New York, 1980).
- [50] National Nuclear Data Center, <https://www.nndc.bnl.gov/nudat3/>.
- [51] C. Rappold and J. López-Fidalgo, *Phys. Rev. C* **94**, 044616 (2016).
- [52] A. S. Botvina, N. Buyukcizmeci, A. Ergun, R. Ogul, M. Bleicher, and J. Pochodzalla, *Phys. Rev. C* **94**, 054615 (2016).
- [53] L. Sheng *et al.*, *Nucl. Instrum. Methods Phys. Res. B* **469**, 1 (2020).
- [54] X. Chen, J. Yang, J. Xia, G. Shen, S. Ruan, G. Wang, J. Liu, J. Zhang, and F. Cai, *Nucl. Instrum. Methods Phys. Res. B* **920**, 37 (2019).
- [55] J. Yang *et al.*, *Nucl. Instrum. Methods Phys. Res. B* **317**, 263 (2013).
- [56] H. Ohnishi, F. Sakuma, and T. Takahashi, *Prog. Part. Nucl. Phys.* **113**, 103773 (2020).
- [57] A. Likar, M. Rosina, and B. Povh, *Z. Phys. A* **324**, 35 (1986).
- [58] O. Hashimoto and H. Tamura, *Prog. Part. Nucl. Phys.* **57**, 564 (2006).
- [59] A. Gal, E. V. Hungerford, and D. J. Millener, *Rev. Mod. Phys.* **88**, 035004 (2016).
- [60] D. Davis, *Nucl. Phys. A* **754**, 3 (2005).
- [61] M. Jurič *et al.*, *Nucl. Phys. B* **52**, 1 (1973).
- [62] E. Botta, T. Bressani, and A. Feliciello, *Nucl. Phys. A* **960**, 165 (2017).
- [63] M. Agnello *et al.*, *Phys. Lett. B* **622**, 35 (2005).
- [64] M. Agnello *et al.*, *Phys. Lett. B* **698**, 219 (2011).
- [65] H. Sagawa, X. R. Zhou, X. Z. Zhang, and T. Suzuki, *Phys. Rev. C* **70**, 054316 (2004).
- [66] H.-J. Schulze, M. Thi Win, K. Hagino, and H. Sagawa, *Prog. Theor. Phys.* **123**, 569 (2010).
- [67] M. May *et al.*, *Phys. Rev. Lett.* **47**, 1106 (1981).
- [68] S. Ajimura *et al.*, *Phys. Rev. Lett.* **86**, 4255 (2001).
- [69] H. Kohri *et al.*, *Phys. Rev. C* **65**, 034607 (2002).
- [70] J. W. Cui, X. R. Zhou, L. X. Guo, and H.-J. Schulze, *Phys. Rev. C* **95**, 024323 (2017).
- [71] W. Y. Li, J. W. Cui, and X. R. Zhou, *Phys. Rev. C* **97**, 034302 (2018).
- [72] H. Mei, K. Hagino, J. M. Yao, and T. Motoba, *Phys. Rev. C* **97**, 064318 (2018).